

Imidazolium-based Ionic liquids on Morphology and Optical Properties of ZnO Nanostructures

A. S. Shahvelayati¹, M. Sabbaghan^{2*} and S. E. Bashtani¹

1. Department of Chemistry, Yadegar-e-Imam Khomeini (RAH) Shahre-rey Branch, Islamic Azad University, Tehran, I. R. Iran.
2. Chemistry Department, Faculty of Sciences, Shahid Rajaee Teacher Training University, Tehran, I. R. Iran.

(*) Corresponding author: sabbaghan@srttu.edu
(Received: 16 Oct 2014 and Accepted: 18 Jan. 2015)

Abstract

ZnO nanostructures have been synthesized by a simple reflux method, using different ionic liquids, such as 1-benzyl-3-methylimidazolium bromide ($[BzMIM][Br]$), 1,1'-(1,4-phenylenebis (methylene)) bis (3-methyl-1H-imidol-3-iun) bromide ($[MM-1,4-DBzIM_2][Br]_2$) and 1-phenacyl-3-methylimidazolium bromide ($[PMIM][Br]$), with different amount of sodium hydroxide in water. Also the effect of reaction time on morphology of ZnO nanostructure using 1-octyl-3-methylimidazolium bromide, $[OMIM][Br]$ is reported. The structure, morphology and optical properties of samples were characterized by means of XRD, SEM and UV-visible absorption. The results show that benzoyl group at position-1 of imidazole ring causes nanosheet ZnO morphology. The time dependent experiments displayed that ZnO nanoparticle arrays and nanosheet ZnO were created. The width and diameter of the resulting ZnO nanosheets can be readily controlled. A possible formation mechanism based on evidence has been discussed. The band gaps are estimated to be 2.57-2.89 eV according to the results of the optical measurements of the ZnO nanostructures. This study shows that ionic liquid may be effect on band gap energy.

Keywords: ZnO, Green synthesis, Nanosheet, Band gap, Ionic liquid.

1. INTRODUCTION

Room temperature ionic liquids (RTILs), especially those based on 1,3-dialkylimidazolium salts, have shown great promise as attractive alternatives to the conventional solvents. RTILs possess the unique advantages of high thermal stability, negligible vapor pressure, immiscibility with both organic compounds and water, and recyclability [1-3]. Ionic liquids (ILs) are important in many industrial processes and green chemistry [4]. Recently, ILs have attracted increasing interest because of their unique properties and potential applications.

ILs can act as templates for the synthesis of inorganic materials with novel or improved properties [5].

Nanostructures of metal oxides have attracted considerable interest in recent years because of their special properties, such as a large surface to volume ratio, high activity, special electronic properties and unique optical properties as compared to those of the bulk materials [6].

Among the metal oxides, much attention has been paid to ZnO for their unique properties, such as electric conductivity,

optical transparency, piezoelectricity and near-UV emission [7-9]. ZnO with a great band (3.3– 3.6 eV) is an important n-type semiconductor, with the large excitation binding energy of 60 meV at room temperature [10-13].

In pursuit of our continuing studies on the development of new routes in approach to the synthesis of ZnO nanostructure, herein, the effect of aryl, benzoyl and alkyl in Imidazolium-based ionic liquids on morphology and optical properties of ZnO nanostructures were investigated [14]. In this research 1-benzyl-3-methylimidazolium bromide abbreviated as ([BzMIM][Br], IL1), dicationic dibromide ionic liquid, 1,1'-(1,4-phenylene bis (methylene)) bis (3-methyl-1*H*-imidazol-3-i^{um}) bromide ([MM-1,4-DBzIM₂][Br]₂, IL2) and 1-phenacyl-3-methylimidazolium bromide ([PMIM][Br], IL3) were used as template. We also explained the effect of reaction time on morphology of ZnO nanostructure using 1-octyl-3-methylimidazolium bromide ([OMIM] [Br], IL4) (Scheme 1). Thus, continuing previous researches leads us to investigate the systematic relationship between the structures of Imidazolium-based ILs and ZnO nanostructures morphology.

2. EXPERIMENTAL

2.1. Synthesis and Characterization of ILs

All the ILs used in this study were synthesized according to Menshutkin reaction [15]. ILs 1-3 syntheses have not been reported hitherto. The IR Spectra were recorded by Shimadzu IR-460 spectrometer. ¹H NMR and ¹³C NMR spectra were measured on Bruker DRX-500 AVANCE instrument in CDCl₃ at 500.1 and 125.7 MHz, respectively δ in ppm, J in Hz. Mass spectra were obtained on a Finnigan MAT-8430 at 70 eV.

1-Benzyl-3-methyl-1*H*-imidazol-3-i^{um} bromide (IL1)

Yellow oil; yield 92%. IR (KBr) (ν_{max} /cm⁻¹): 3065, 2853, 1570, 1454, 1161, 722, 621. ¹H NMR: δ = 3.83 (3 H, s, Me), 5.43 (2 H, s, CH₂), 7.32-7.42 (5 H, m, 5 CH-), 7.72 (1 H, dd, 3J = 1.7, 4J = 1.7, CH), 7.81 (1 H, dd, 3J = 1.7, 4J = 1.7, CH), 9.34 (1 H, s, CH) ppm. ¹³C NMR: δ = 36.7 (Me), 52.6 (CH₂), 123.2 (CH), 124.8 (CH), 129.2 (2 CH), 129.5 (CH), 129.8 (2 CH), 135.8 (C), 137.5 (CH) ppm.

1,1'-(1,4-Phenylenebis(methylene)) bis(3-methyl-1*H*-imidazol-3-i^{um}) bromide (IL2)

White powder, mp 224-226°C; yield 93%. IR (KBr) (ν_{max} /cm⁻¹): 3065, 2952, 1577, 1558, 1174, 865, 753, 620. ¹H NMR: δ = 3.82 (6 H, s, 2 Me), 5.42 (4 H, s, 2 CH₂), 7.37-7.52 (4 H, m, 4 CH-Aromatic), 7.71 (2 H, dd, 3J = 1.7, 4J = 1.7, 2 CH), 7.77 (2 H, dd, 3J = 1.7, 4J = 1.7, 2 CH), 9.29 (2 H, s, 2 CH) ppm. ¹³C NMR: δ = 36.5 (2 Me), 52.4 (2 CH₂), 123.3 (2 CH), 124.5 (2 CH), 128.6 (4 CH), 134.9 (2 C), 137.6 (2 CH) ppm.

3-Methyl-1-(2-oxo-2-phenylethyl)-1*H*-imidazol-3-i^{um} bromide (IL3)

Pale yellow powder, mp 104-107 °C; yield 95%. IR (KBr) (ν_{max} /cm⁻¹): 3084, 1697, 1562, 1226, 1162, 753, 691. ¹H NMR: δ = 3.95 (3 H, s, Me), 6.11 (2 H, s, CH₂), 7.62 (2 H, t, 3J = 7.5, 2 CH), 7.74 (1 H, s, CH), 7.75 (1 H, t, 3J = 7.5, CH), 7.80 (1 H, s, CH), 8.05 (2 H, d, 3J = 7.5, 2 CH), 9.13 (1 H, s, CH) ppm. ¹³C NMR: δ = 38.6 (Me), 58.9 (CH₂), 123.5 (CH), 124.7 (CH), 127.9 (2 CH), 133.4 (CH), 134.6 (2 CH), 135.3 (C), 137.7 (CH), 193.5 (C=O) ppm. EI-MS: m/z (%) = 283 (M+2, 6), 281 (M+1, 6), 236 (25), 208 (22), 150 (20), 137 (18), 105 (95), 82 (100), 71 (40), 57 (50).

1-Octyl-3-methylimidazolium bromide (IL4)

Yellow oil; yield 92%. ¹H NMR: δ = 0.78 (3 H, t, 3J = 6.1, Me), 1.16-1.24 (10 H, m, 5 CH₂), 1.82-1.85 (2 H, m, CH₂), 3.81 (3 H, s,

CH_3), 4.16-4.13 (2 H, t, $^3J = 7.1$, CH_2), 7.43 (1 H, dd, $^3J = 1.7$, $^4J = 1.7$, 1 CH), 7.61 (1 H, dd, $^3J = 1.7$, $^4J = 1.7$, 1 CH), 10.26 (1 H, s, CH) ppm.

2.2. Synthesis and Characterization nanostructures of ZnO

Zinc acetate dihydrate was purchased from Aldrich. Sodium hydroxide was used without further purification. The definite amount of NaOH was dissolved in 30 mL of distilled water under vigorous stirring, followed by the addition IL (4mmol) and 0.3 g $\text{Zn}(\text{AcO})_2 \cdot 2\text{H}_2\text{O}$ to the mixture. The mixture transferred to a round bottom flask and was refluxed in definite time. After cooling to room temperature, the precipitate was collected by filtration and washed with acetone, distilled water and ethanol (96%) several times. Finally, the ZnO samples were obtained by centrifugation and drying of the precipitate in the air at room temperature. Also time dependent experiment was done with IL4. The experimental conditions, morphologies and crystallite particle size of samples were listed in Table 1.

The morphology of nanostructure ZnO was determined by using scanning electron microscopy (SEM) of a Holland Philips XL30 microscope. X-ray diffraction (XRD) analysis was carried out at room temperature using a Holland Philips Xpert X-ray powder diffractometer with Cu Ka radiation ($\lambda = 0.15406 \text{ nm}$), over the 20 collection range of 20-80°. Average crystallite sizes of products were calculated using Scherrer's formula: $D = 0.9\lambda/\beta \cos \theta$, where D is the diameter of the nanoparticles, $\lambda (\text{Cu Ka}) = 1.5406 \text{ \AA}$ and β is the full-width at half-maximum of the diffraction lines.

The band gaps of samples were determined by a UV-visible spectrometer on an instrument PG T80/T80⁺ with drift and solid cells. The spectra were recorded at room temperature in the wavelength range of 200-800nm and with the accuracy of 0.5nm.

3. RESULTS AND DISCUSSION

3.1. Structure and morphology

3.1.1. Morphologies of samples 1-6.

The morphologies of ZnO nanostructures prepared in ILs 1-3 under different conditions are shown in Figure 1. Using IL1 and IL2 as template, ZnO nanopaticles with cristalize size between 20-32 nm were obtained. ZnO nanoparticle was synthesized in ratio of 4:1 $\text{NaOH}/\text{Zn}(\text{OAc})_2 \cdot 2\text{H}_2\text{O}$. ZnO in IL3. By changing ratio of $\text{NaOH}/\text{Zn}(\text{OAc})_2 \cdot 2\text{H}_2\text{O}$ to 2:1, nanosheet morphology was obtained. Each nanosheet structure has a diameter of about ~28nm, a length of ~270nm and width ~225nm.

The XRD pattern of the as-obtained products is shown in Figure 2. All the prominent peaks in the pattern correspond to the wurtzite structure of ZnO, which can be indexed on the basis of JCPDS file no. 36-1451. The results indicate that the products consist of pure phases and no characteristic peaks are observed for other impurities, such as $\text{Zn}(\text{OH})_2$. Moreover, no remarkable shift of the diffraction peaks among the samples reveals that lattice expansion and/or shrinkage can be neglected. In fact, if we look at the XRD patterns deeply, we observe that all samples exhibit high relative intensities for the (1 0 1) peak revealing a preferred orientation of their corresponding products. While comparing with other peaks, the samples show different relative intensities of the (0 0 2) peak. The average crystal sizes were calculated from the FWHM in XRD pattern using Debye-Scherrer's equation and listed in Table 1. It is found that the average crystal sizes reduced with using the IL1, IL2 and IL3 compared to without IL sample [14].

3.1.2. Morphologies of samples 7-9.

The time-dependent experiments were performed in IL4, with ratio 4:1 of $\text{NaOH}/\text{Zn}(\text{OAc})_2 \cdot 2\text{H}_2\text{O}$ at different times (30 min., 1.5 h and 16 h). These samples are named 7, 8, 9 (Table 2). The XRD pattern

and SEM are shown in Figure 3. The mixture of nanoparticle and nanosheet were obtained after 30 minutes. As reported in our previous article, uniform nanosheet ZnO synthesized after 1.5 h [14]. With increasing the reflux time to 16 h, the width and diameter of ZnO nanosheets increased. These nano-sheets have the diameter of ~66 nm, length of ~700nm and the width of

~375nm. Therefore, width and diameter of nanosheet can be easily controlled by changing IL and reflux time. The XRD patterns of samples 7-9 show the wurtzite structure of ZnO which no characteristic peaks are observed for other impurities in them (Figure 3).

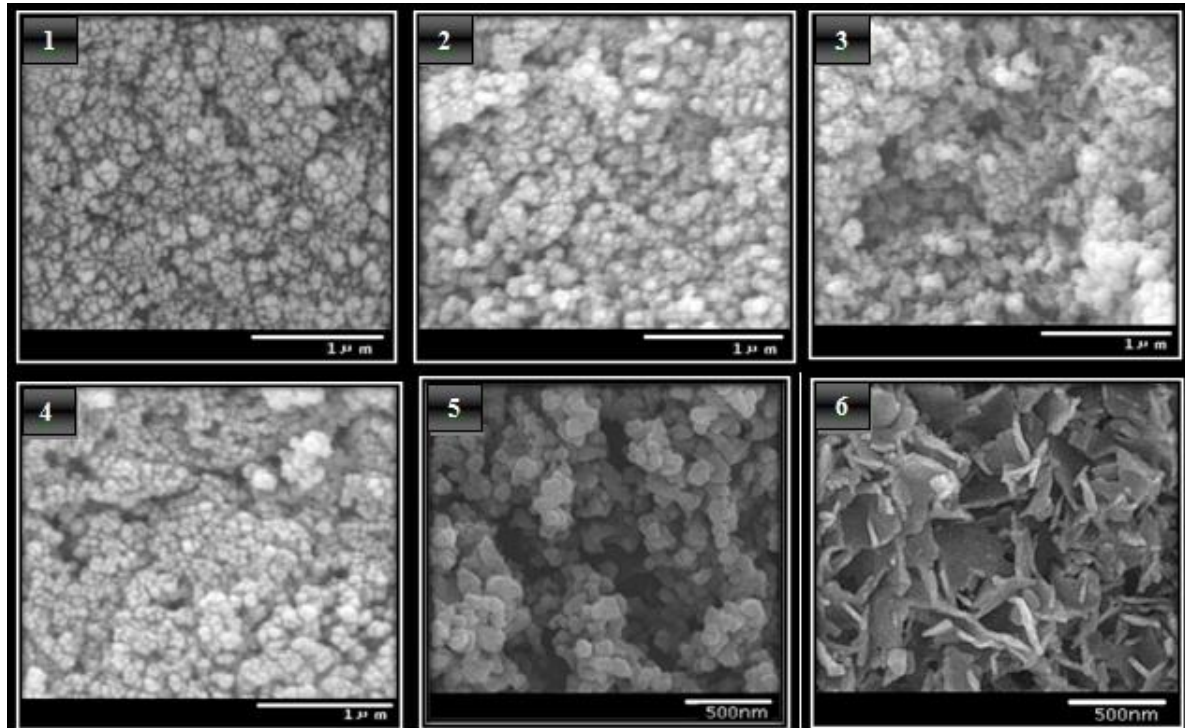
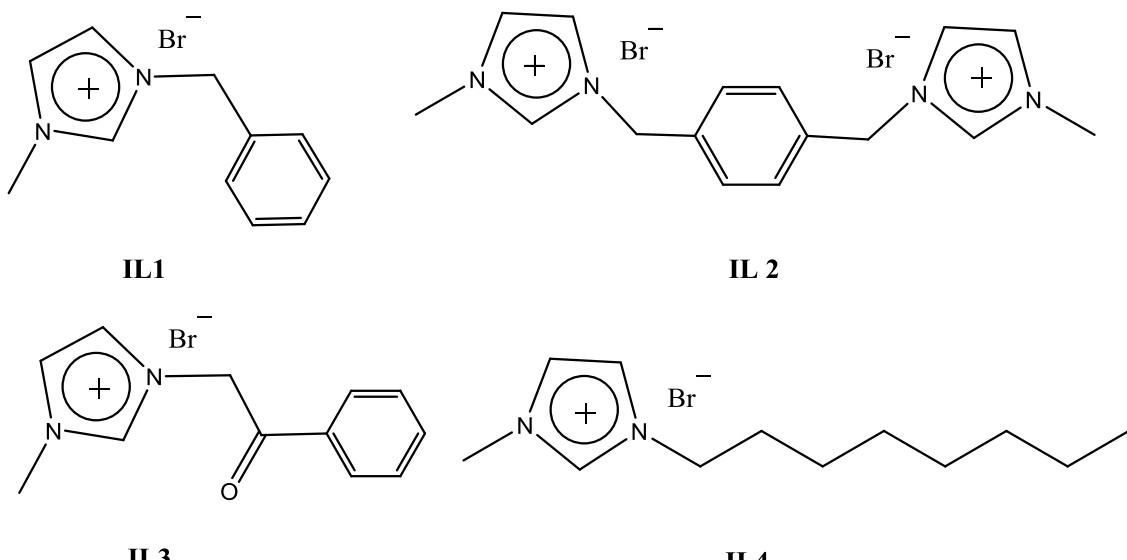


Figure 1. SEM images of ZnO nanostructures.



Scheme 1. Chemical structures of Ionic Liquid.

Table 1. Preparation of ZnO nanostructures by reflux method in water with information on morphology and crystallite particle size, (NP: nanoparticle, NS: nanosheet)

Sample	NaOH/Zn(OAc) ₂ .2H ₂ O	IL	Morphology	Time	Size (nm)
1	4:1	1	NP	1.5	23
2	2:1	1	NP	1.5	21
3	4:1	2	NP	1.5	21
4	2:1	2	NP	1.5	32
5	4:1	3	NP	1.5	20
6	2:1	3	NS	1.5	32
7	4:1	4	NS & NP	0.5	18
8	4:1	4	NS	1.5	28
9	4:1	4	NS	16.0	28

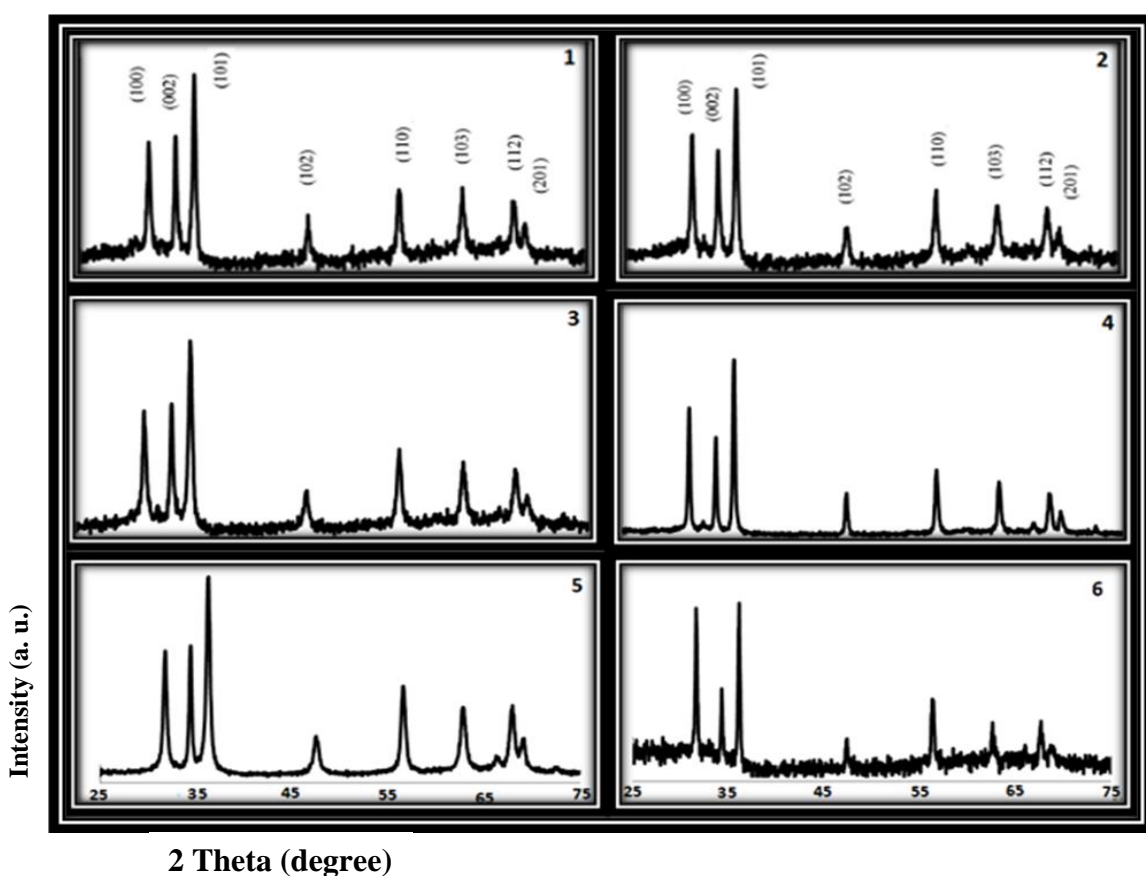


Figure 2. XRD pattern of ZnO nanostructures.

3.2. Possible mechanism of formation

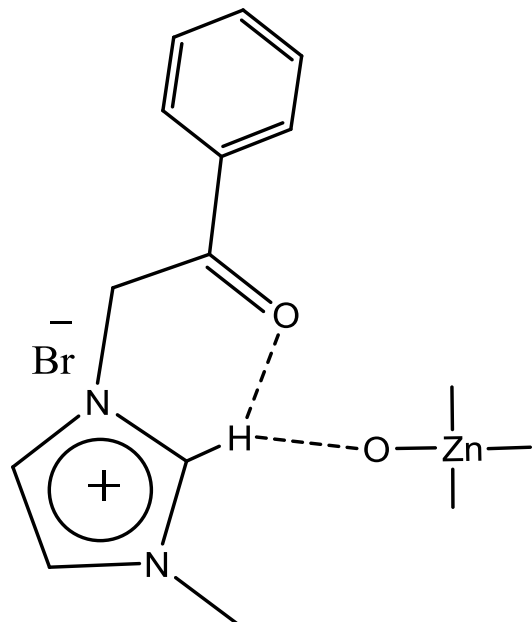
The growth unit for ZnO crystal is considered to be Zn(OH)₄²⁻ [16]. Imidazolium ion can combine with [Zn(OH)]²⁻ through the electrostatic attraction [14]. This complex gets dehydrated quickly and is converted to ZnO.

The study of the effect of IL1 and IL2 on the morphology of the ZnO nanostructures show that the benzyl group at position-1 of

imidazolium cation causes steric hindrance and decrease of interaction between “nucleus” and C(2)-H of imidazolium ring. These results showed that the interactions between ZnO surface and ionic liquid are less compared to IL3 and IL4. IL1 and IL2 act as a dispersant and didn't play an important role in morphology control of ZnO nanostructures.

In the case of IL3, nanosheet ZnO were synthesized in 2:1 and nanoparticle ZnO in

4:1 ratio of NaOH/Zn(OAc)₂.2H₂O. It seems intermolecular hydrogen bond of C(2)-H and carbonyl group in the presence of excess NaOH is enhanced. On the contrary, the hydrogen bond, formed between the hydrogen atom at position 2 of the imidazole ring and the oxygen atoms of O-Zn can be weak in this condition (Scheme 2). The results revealed that the IL with intermolecular hydrogen bond and the amount of base can induce the preferential growth of ZnO crystal nuclei in a certain direction.



Scheme 2. Hydrogen bonds in IL3.

Also time-dependent experiments in IL4 indicated that ZnO nanoparticle arrays and nanosheet ZnO were created.

3.3. Optical properties

To study the effect of ILs on the band gap of the ZnO nanostructures, the UV-vis absorption spectra of all the samples 1-6 were studied, which are shown in Figure 4. Excitonic absorption peaks are observed at 391, 393, 388, 404, 391, and 385 nm for the samples 1-6 respectively (Table 2). Absorption peak of sample without template, reported in the previous article, was appeared at 349 nm [14]. A clear red-shift in the absorption peak is observed compared with no IL sample.

The band gap energies can be estimated in according to the following equation [17]:

$$\alpha E_{\text{photon}} = K(E_{\text{photon}} - E_g)^{1/2}$$

Where K is a constant, α is the absorption coefficient, E_{photon} is the discrete photo energy and E_g is the band gap energy. The energy intercept of a plot of $(\alpha E_{\text{photon}})^2$ vs. E_{photon} yields E_g for a direct transition. The value of band gap energies present in Table 2. The red shift of the band gap using ILs has been observed and effectively extends the absorption edge into the visible region. Also these values are smaller than the reported value for bulk ZnO ($E_g = 3.4$ eV) [18].

To study the effect of reflux time on the band gap of ZnO nanostructures, the UV-vis absorption spectra and band gap of the samples 7-9 were studied which are shown in Figure 4 and Table 2. The band gap of ZnO is decreased with an increase in reflux time. This is due to the increase in particle size of ZnO with reflux time. Also IL may influence band gap energy.

Table 2. Physicochemical characteristics of ZnO nanostructures.

Sample	Absorption peak (nm)	Band gap energy (eV)
1	391	2.72
2	464	2.74
3	478	2.72
4	453	2.57
5	485	2.70
6	475	2.68
7	432	2.89
8	430	2.88
9	450	2.75

Figure 5 shows band gap of ZnO particles as a function of particle size for samples 1-5. Although all of these samples are nanoparticles of ZnO, they have no the same band gaps. It seems the IL structure can be effect on band gap energy.

4. CONCLUSION

Herein, the effect of various substitution in imidazolium base ionic liquids on morphology and optical properties of synthesized nano ZnO are investigated in reflux condition. The present work

demonstrates that intramolecular hydrogen bond and steric effect on imidazolium based ILs as the template have important role on morphology of ZnO nanostructures.

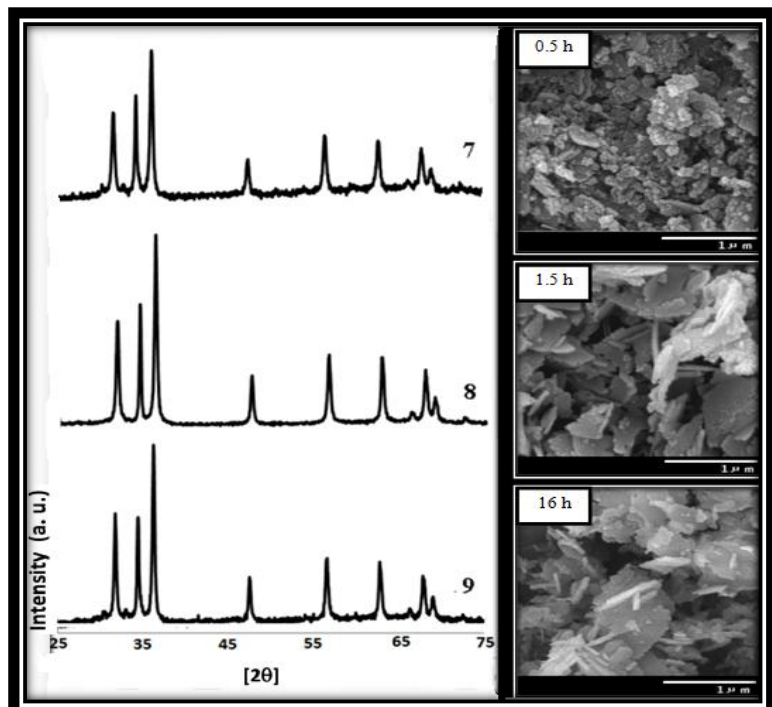


Figure 3. SEM and XRD of samples in time dependent experiments.

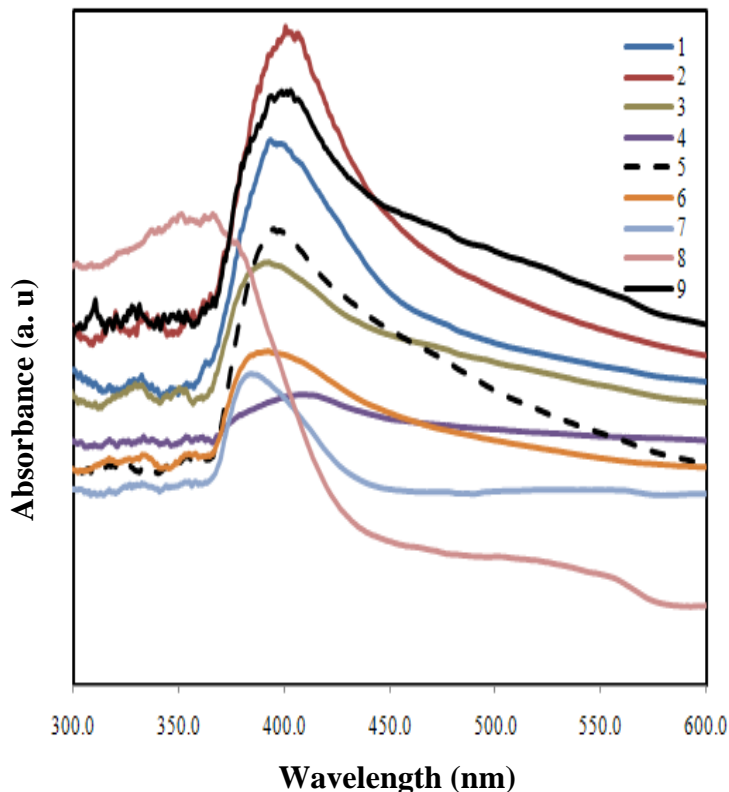


Figure 4. UV-vis spectra of ZnO nanostructures.

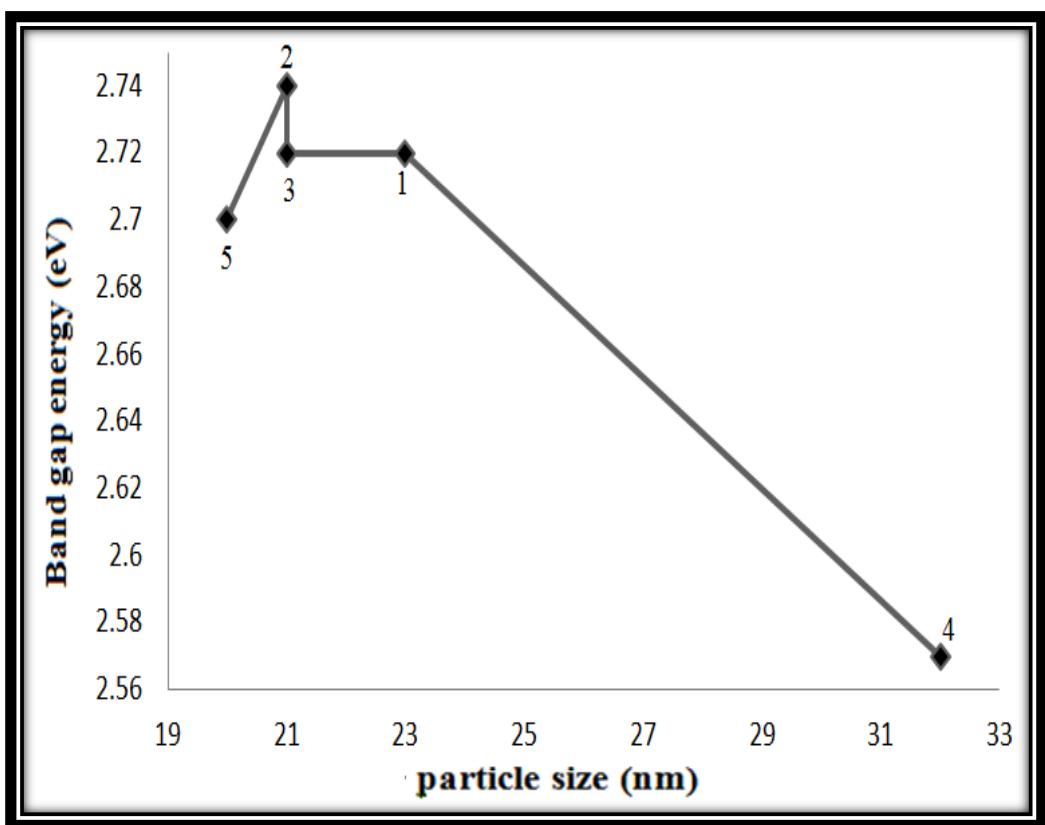


Figure 5. Band gap of ZnO particles as a function of particle size.

The time-dependent experiments in 1-octyl-3-methylimidazolium bromide as the template indicated that ZnO nanoparticle arrays and nanosheet ZnO were created. The UV-vis spectra of the resultant samples indicate red-shift in the absorption peak compared with bulk ZnO. The band gap of ZnO is decreased with increasing the reflux time, and λ_{\max} is also shifted to higher wavelengths. This research by following the previous articles can be useful to get a deeper understanding of ILs behavior mechanism in ZnO nanostructures synthesis.

REFERENCES

- P. Wasserscheid, T. Welton, Ionic liquids in synthesis, Weinheim: Wiley, (2003).
- I. Yavari, E. Kowsari: Tetrahedron Lett., Vol. 48, No. 21, (2007), pp. 3753-3756.
- I. Yavari, A.S. Shahvelayati, M. Ghanbari, M. Ghazvini, M. Piltan: J. Iran. Chem., Soc. Vol. 8, No. 3, (2011), pp. 636-642.
- H. Zhao: Chem. Eng. Commun., Vol. 193, No. 12, (2006), pp. 1660–1677.
- A. Taubert: Angew. Chem. Int'l. Ed. Engl., Vol. 43, No. 40, (2004), pp. 5380–5382.
- T. Alammar, A. Birkner, O. Shekhah, A.V. Mudring: Mater. Chem. Phys., Vol. 120, NO. 1, (2010), pp. 109–113.
- T. Kawano, H. Imai: Colloids Surf. A., Vol. 319, No. 1-3, (2008), pp. 130–135.
- C.C. Chen, P. Liu, C. Lu: Chem. Eng. J., Vol. 144, No. 3, (2008), pp. 509–513.
- L. Tang, B. Zhou, Y. Tian, H. Bala, Y. Pan, S. Ren, Y. Wang, X. Lv, M. Li, Z. Wang: Colloids Surf. A., Vol. 296, No. 1-2, (2007), pp. 92–96.

10. Y.S. Kim, W.P. Tai, S.J. Shu: Thin Solid Films, Vol. 491, No. 1-2, (2005), pp. 153–160.
11. M. Li, H. Bala, X. Lv, X. Ma, F. Sun, L. Tang, Z. Wang: Mater. Lett., Vol. 61, No. 3, (2007), 690–693.
12. R. Liu, A.A. Vertegel, E.W. Bohannan, T.A. Sorenson, J.A. Switzer: Chem. Mater. Vol. 13, No. 2, (2001), pp. 508-512.
13. [P. Uthirakumar, B. Karunagaran, S. Nagarajan, E.K. Suh, C.H. Hong: J. Cryst. Growth., Vol. 304, No. 3, (2007), pp. 150–157.
14. M. Sabbaghan, A.S. Shahvelayati, S. E. Bashtani: Solid State Sci., Vol. 14, No. 10, (2012), pp. 1191-1195.
15. U. Sola, A. Lledos, M. Duran, J. Bertran, J. L. M. Abboud: J. Am. Chem. Soc., Vol. 113, No. 8, 1991, pp. 2873–2879.
16. W. J. Li, E. W. Shi, W. Z. Zhong, Z. W. Yin: J. Cryst. Growth., Vol. 203, No. 1-2, (1999), pp. 186–196.
17. Y. Hu, H. J. Chen: Nanopart. Res., Vol. 10, No. 8, (2008), pp. 401–407.
18. R. Shi, P. Yang, X. Dong, Q. Ma, A. Zhang: Appl. Surf. Sci., Vol. 264, (2013), pp. 162–170.
19. S. Dhara, P. K. Giri: Appl Nanosci., Vol. 1, No. 4, (2011), pp. 165–171.
20. A. B. Djurisic, and Y. H. Leung: Small, Vol. 2, No.8-9, (2006), pp. 944 – 961.